Harnessing Peptide Binding to Capture and Reclaim Phosphate

Whitney C. Fowler,[†] Chuting Deng,[†] Gabriella M. Griffen,[†] Tess Teodoro,[†] Ashley Z. Guo,[†] Michal Zaiden,[§] Moshe Gottlieb,[*,§] Juan J. de Pablo,[*,†,‡] Matthew V. Tirrell[*,†,‡]

[†] Pritzker School of Molecular Engineering, University of Chicago, Chicago, Illinois 60637, United States,

[§] Chemical Engineering Department, Ben-Gurion University, Beer Sheva 841050, Israel,

[‡] Argonne National Laboratory, Lemont, Illinois 60439, United States.

Keywords: Resource recovery, capture and release material, biomimetic material, phosphate recovery, computer simulations, free energy mapping

ABSTRACT: With rising consumer demands, society is tapping into wastewater as an innovative source to recycle depleting resources. Novel reclamation technologies have been recently explored for this purpose, including several that optimize natural biological processes for targeted reclamation. However, this emerging field has a noticeable dearth of synthetic material technologies that are programmed to capture, release, and recycle specified targets; and of the novel materials that do exist, synthetic platforms incorporating biologically inspired mechanisms are rare. We present here a prototype of a materials platform utilizing peptide amphiphiles that has been molecularly engineered to sequester, release, and reclaim phosphate utilizing a stimuli-responsive pH trigger, exploiting a protein-inspired binding mechanism that is incorporated directly into the self-assembled material network. This material is able to sequester and controllably release phosphate for multiple cycles of reuse, and it is selective over nitrate and nitrite. We have determined by simulations that the binding conformation of the peptide becomes constrained in the dense micelle corona at high pH such that phosphate is expelled when it otherwise would be preferentially bound. However, at neutral pH, this dense structure conversely employs multi-chain binding to further stabilize phosphate when it would otherwise be unbound, opening opportunities for higher-order conformational binding design to be engineered into this controllably packed corona. With this work, we are pioneering a new platform to be readily altered to capture other valuable targets, presenting a new class of capture and release materials for recycling resources on the nanoscale.

1. Introduction

As critical resources are being unsustainably depleted while the global demand increasingly rises, society is turning towards wastewater as a new source for reclaiming valuable products or toxic chemicals,[1–4] including rare metals,[5] critical fertilizer ingredients,[6] and pharmaceutical products.[7,8] Our ability to harvest these, however, is limited by several infrastructural, societal, and technological challenges.[1] In particular, the emerging field of resource reclamation lacks versatile materials that are molecularly engineered to recognize, capture, and release their targets in a controllable and practical manner.

A promising design scheme in this endeavor is to exploit the inherent ability of proteins to specifically recognize, bind, and release their target molecules and incorporate this function into a tunable synthetic material. Natural abilities of phosphate-processing organisms have been harnessed in their raw form to reclaim phosphorus,[9] including the prokaryotic processes of enhanced biological phosphorus removal or eukaryotic technologies such as floating algae farming. A challenge for these technologies is that of grappling with complex operating conditions required for optimized resource reclamation.[6,9–12] On a larger scale, engineered wetlands systems have also been employed to reclaim nutrients, but thus far they have not gained momentum in use due to a limited resource return rate.[10] Since these technologies employ organisms in their raw form, they face the innate restrictions imposed by the organism's metabolism, thereby restricting opportunities for optimization. This unique biological sequestering ability could be fully realized if it were intentionally designed into a synthetic materials platform. However, attempts to develop a hierarchically driven, biomimetic materials design scheme for resource capture and release have been limited.

A strategic target compound for development of a prototype capture-and-release material is phosphate, a commodity widely targeted by other technologies in addition to those described above.[6,9–17] This limited resource is an essential ingredient in many fertilizers,[18,19] but at its current rate of extraction, it is projected to be expended in 50 to 100 years.[20] Paradoxically, this highly coveted resource is also being discarded in large amounts in agricultural runoff streams, thereby causing severe eutrophication and vastly disrupting natural ecosystems.[21] An effective, capture-and-release material could be strategically employed to target and recover phosphate from where it is detrimental and reinsert it where it is depleted yet greatly needed.

In this work, we present a prototype of a novel materials platform that relies on self-assembled peptide amphiphiles to controllably capture, release, and reclaim phosphate through a pH-responsive trigger, exploiting the natural binding ability of proteins. Peptide amphiphiles (PAs) consist of a short peptide sequence "headgroup" conjugated to a hydrophobic "tail" that causes spontaneous self-assembly into micelles in water.

The PAs can be precisely designed and synthesized to feature multiple functional "building block" segments,[22,23] such as protein-derived binding amino acid sequences that are systematically displayed upon assembly in the micelle coronae,[24] or segments to promote protein secondary structure conformations in the headgroup,[25] a well-known critical component in biological binding. Indeed, PAs have previously harnessed this specific targeting ability of biological molecules for use in targeted drug delivery[26,27] and cell adhesion,[28] making this platform well-positioned to transition in application towards specified targeting of selected resources. Along those lines, PAs have recently been studied for macromolecular harvesting of proteins,[29] which exploits similar concepts but could have differences in its practical implementation due to molecular size and transport phenomena. Our material design is easily accomplished through use of well-studied, sequence-specific synthesis techniques to produce environmentally benign materials, an advantage over other novel capture and release materials such as metal organic frameworks that have complex synthetic routes, can be toxic, and are unstable in water.[30–32]

In addition to exploiting advantages in synthesis and targeted binding, we also leveraged the unique material characteristics of PAs, showing the importance of control over multiple length scales. In our work, the micelle architecture of PA spontaneous self-assembly was tuned according to well-studied strategies to direct the PAs towards self-assembly into wormlike micelles that form an entangled, dense suspension.[33] This network hosts a multitude of phosphate-binding sites on its exposed surfaces and provides a physical structure through which phosphate-rich water can flow, capturing the phosphate ions on the strands of the network. The ions can later be controllably released by a pH trigger. The self-assembled network thereby inherently offers a practical means to reclaim this valuable resource. To develop the proposed materials and gain a mechanistic understanding of the molecular processes through which phosphate is captured, we have relied on molecular simulations of the molecules and self-assembled structures of interest. Although the initial prototype will target phosphate, the versatility and breadth of PAs positions us to modify peptide binding sequences to target, sequester, and reclaim, with potentially high avidity and selectivity, a large number of other valuable resources such as heavy metals, pharmaceuticals, or bioplastics, with the potential to truly become a modular materials platform for wastewater resource recovery.

2. Results and Discussion

2.1 Design of the Peptide Amphiphile Prototype Material

With strategic design from the molecular level up, each PA molecule can be individually tuned to dictate its bulk self-assembled and phosphate binding properties (Figure 1). Here, we designed two different molecules to evaluate, denoted C_{16}GGGhex and C_{16}SGKGHhex, each consisting of three key design regions intended to optimize both functionalities: (1) producing wormlike micelles to create an entangled network and (2) optimizing phosphate binding performance. Each of these molecules was synthesized using FMOC solid phase peptide synthesis with precise monodisperse control and promise in scalability.[34]

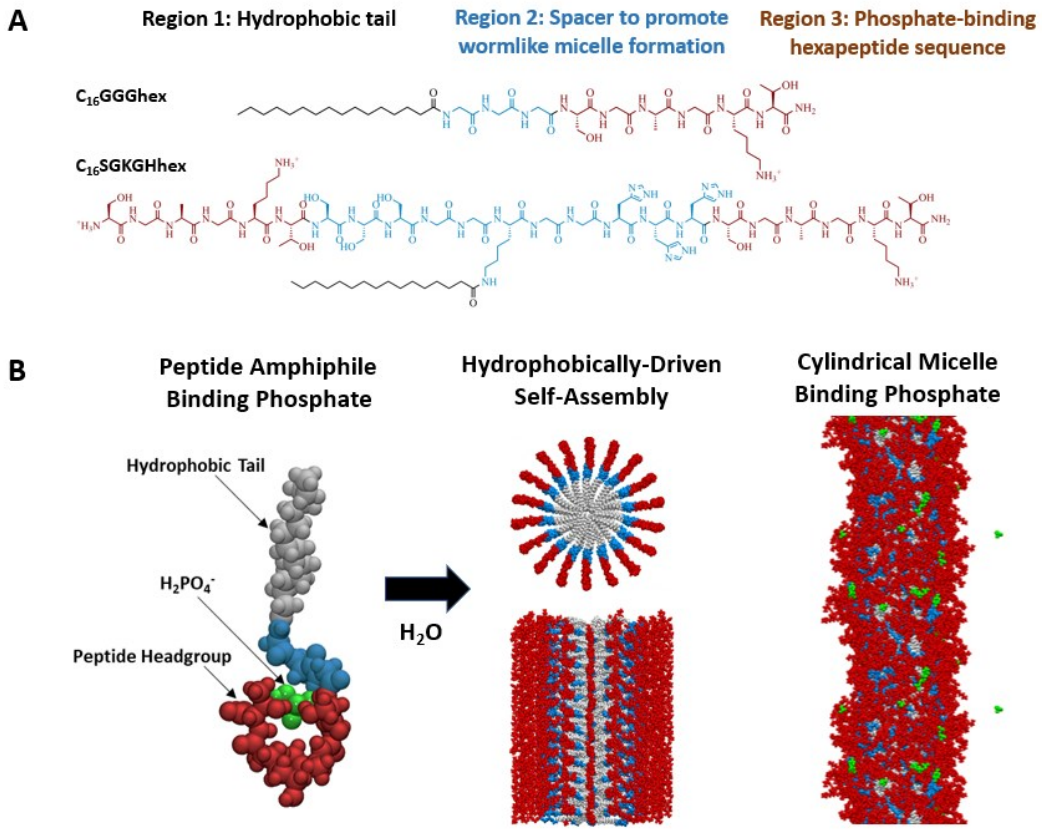

Figure 1. (A) PAs denoted C_{16}GGGhex andC_{16}SGKGHhex. (B) Simulation snapshots of C_{16}GGGhex. On the left, an individual PA binds to a phosphate ion in the peptide headgroup through utilizing the P-loop mechanism of hydrogen bonds of the peptide backbone and nested cavity promoted by the side chain lysine. When submerged in water, the PAs spontaneously self-assemble into a micelle to shield the cores from the aqueous solution (middle). The PA micelle binds to phosphate in the corona (right).

The critical binding moiety of our material platform (Region 3) is the protein-derived phosphate-binding sequence that protrudes into the aqueous environment, coating the surface area of the entangled wormlike micelle network with readily accessible binding sites for phosphate. The phosphate binding of proteins has been thoroughly studied in other works,[35,36] but here we extract a specific well-known sequence to molecularly engineer a new system for targeted harvesting of phosphate in a self-assembled network. The binding sequence we chose, namely SGAGKT, is taken from the P-loop motif which is common in phosphate-binding proteins. It consists of a sequence of GXXXXGK[S,T], where X is any amino acid residue and the final residue is either serine or threonine.[37] The P-loop motif stabilizes the phosphate group of proteins, commonly of ATP or GTP, by creating a nest around the phosphate of hydrogen bonds from the amines in the P-loop backbone and utilizing the positively charged lysine side chain, as depicted in Figure 1. We selected this specific SGAGKT hexapeptide binding sequence because it was a commonly repeated motif among myosin-heavy chains, as opposed to other P-loop sequences that had more variation between proteins,[37] and it was previously synthesized and found to bind phosphate in a pH-dependent manner.[38,39]

Equally essential to our material design is Region 1 of the PA, the "tail" which drives the PAs to self-assemble according to the hydrophobic effect, driving the hydrophilic peptide "headgroup" to be systematically displayed to the environment in the micelle corona. For both molecules, we selected the tail to be palmitic acid (C_{16}) for its use in previous systems that adopted a wormlike micellar assembly.[40]

Finally, we incorporated Region 2 of our PAs, which we call the "spacer" here, for two purposes: i) to extend the binding moiety further into the aqueous solution and thus make the binding pocket more accessible, and ii) to produce intramolecular hydrogen bonding that in turn induces wormlike micelle formation, the desired architecture for our entangled material design. For the latter purpose, we tested two designs. The "GGG" in the name C_{16}GGGhex corresponds to three glycine residues between the tail and the binding sequence, which have been shown previously to produce hydrogen bonded beta sheets that encourage the assembly into a wormlike micellar structure.[41] Similarly, the "SGKGH" notation for C_{16}SGKGHhex corresponds to serine, glycine, and histidine residues on either side of the lysine, whose side chain amine is used to construct the branched PA junction through its direct conjugation to the tail. This double-headed branched design, without the hexapeptide, was previously shown to promote crosslinked, self-supported gelation at pH > 6.5 due to hydrogen bonding between the hydroxyl groups of the serine residues and the deprotonated imidazole side chains of the histidine residues.[40] It was chosen here with the intent to further increase the robustness of our entangled wormlike micelle network through these engineered physical crosslinks. Thus, by keeping PA design Regions 1 and 3 constant, we could directly evaluate the impact of each strategy for hydrogen bonding in Region 2 on the two overall design aims of (1) producing a robust wormlike micelle network and (2) optimizing phosphate binding performance.

2.2 Analysis of Self-Assembled Micelle Properties

To characterize our capture-and-release material, we first analyzed the self-assembly properties of the PAs. To begin, we measured the critical micelle concentration (CMC), that is, the concentration at which the PAs begin to self-assemble. The CMCs were 8.43 μM and 130.1 μM for C_{16}GGGhex and C_{16}SGKGHhex, respectively (Figure S3). These values are in the expected range for PA molecules, but this ten-fold difference is noteworthy and is explained by the packing parameter, *P*, for these amphiphilic molecules. *P* relates the chemistry of the molecule, most notably the area of the headgroup, to the packed self-assembled state (see SI for further discussion).[42] In our binding materials, the lower CMC value of C_{16}GGGhex is advantageous because it corresponds to a lower concentration of unimer PAs in solution when the system is assembled above the CMC. To minimize the ratio of unimer to assembled micelle and to ensure that we are always working with assembled materials, we conducted all future experiments at a concentration of PA at least 10 times greater than the value of the CMC, unless otherwise noted.

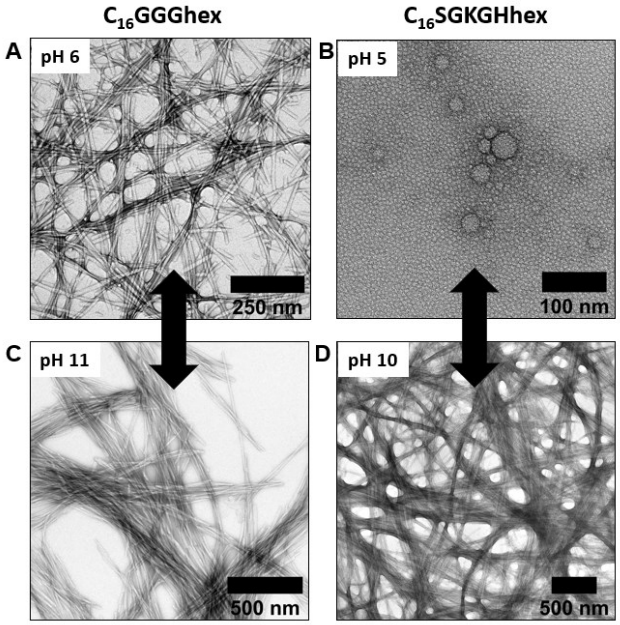

Figure 2. TEM images of C_{16}GGGhex and C_{16}SGKGHhex at neutral and high pH values. Both systems exhibit a reversible pH micelle transition when switching from neutral/acidic to high pH. C_{16}GGGhex clumps together at high pH, while C_{16}SGKGHhex assembled into spheres at pH 5 and clumped wormlike micelles at high pH.

We performed negative stain transmission electron microscopy (TEM) to visualize the micellar architectures and calculate the length scales of the micelle assemblies. For each system, we see a pH dependence of micelle formation. For C_{16}GGGhex, we observe entangled wormlike micelles with an average diameter of 11.5 nm that extend tens of microns in length at neutral pH (Figure 2A).[43] This is the desired micelle architecture for our capture and release material to provide a solid support through which phosphate-rich solution can flow. At high pH (Figure 2C), we observe that the wormlike micelles cluster together. This phenomenon is likely due to the lysine side chain being deprotonated, resulting in assemblies that are less soluble and then stabilize through aggregation. This pH-dependent aggregation is reversible (Figure S8). Overall, C_{16}GGGhex is well-suited to form a dense suspension for the retention and release of phosphate.

For C_{16}SGKGHhex, we also observe reversible pH dependence on micelle formation. At pH 5 and below, C_{16}SGKGHhex assembles into spherical micelles with a diameter 7.2 nm (Figure 2B), but by pH 10, it has transitioned into wormlike micelles that are also clumped together and extend for tens of microns (Figure 2D). This transition from sphere to wormlike micelles has been noted previously for pH-dependent materials.[44,45] For C_{16}SGKGHhex, the effective headgroup area decreases when the histidine imidazole groups are deprotonated at high pH, reversibly pushing the assembly to be most stabilized as wormlike micelles. Overall, this PA micelle platform showcases the unique tunability of small molecular variations on microscale properties, and though it does not produce the desired entangled network for the full pH range, it will allow us to determine how this micelle shape transition affects binding.

2.3 Analysis of Fundamental Phosphate-Binding Properties

We evaluated and compared the phosphate binding functionality of the two PA micelles. We employed a spectrophotometric assay to quantify phosphate binding which emits a blue color linearly proportional to the amount of phosphate in solution.[46,47] To perform the binding process, we combined the phosphate and PA at the desired concentrations, adjusted the pH using minimal HCl and NaOH, physically separated the PA from the unbound phosphate in solution, and then performed the spectrophotometric assay on the filtrate containing unbound phosphate. The PO_4 feed concentration was chosen to be 0.5mM (47.5ppm) for all experiments to simulate a comparable phosphate concentration to that of municipal wastewater influent streams.[48] For this preliminary fundamental testing, we evaluated the phosphate binding dependence on three factors: (i) the pH of the solution, (ii) the ratio of the hexapeptide binding unit to phosphate, and (iii) length of time permitted to bind.

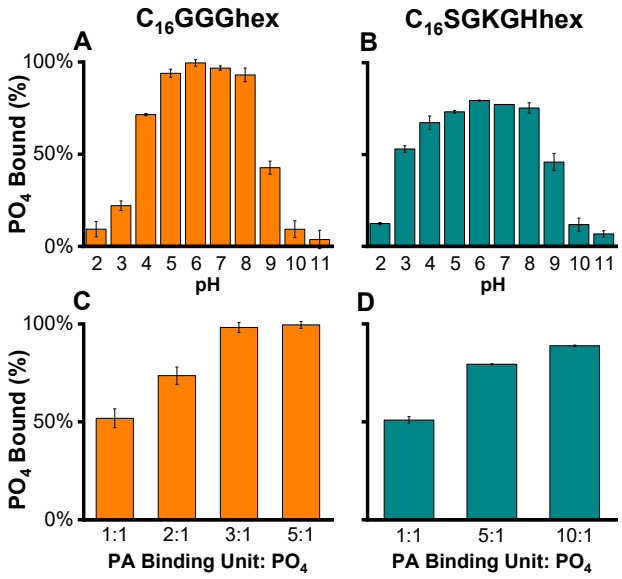

Figure 3. (A-B) pH-dependent phosphate binding of the PA micelles (A) C_{16}GGGhex and (B) C_{16}SGKGHhex at a molar ratio of 5:1 PA binding unit: PO_4 and a PO_4 feed concentration of 0.5 mM (47.5 ppm). For C_{16}GGGhex, essentially 100% of phosphate (within measurement error) was bound to the micelle at pH 6, representing the ideal "capture" conditions, while only 5% and 10% of PO_4 was bound at pH 2 and 10, respectively, becoming ideal "release" conditions. For C_{16}SGKGHhex, a similar trend of maximum and minimum binding was observed, although complete binding was not achieved. (C-D) Phosphate binding at pH 6 when the ratio of PA binding unit: PO_4 was varied while keeping the concentration of PO_4 constant at 0.5 mM. (C) For C_{16}GGGhex, 92% and 100% of binding were achieved at a ratio of 3:1 and 5:1 PA binding unit: PO_4, respectively. (D) For C_{16}SGKGHhex, only 89% binding was achieved even when the ratio was increased to 10:1.

The results in Figure 3 depict how phosphate binding depends on pH and the ratio of binding unit to phosphate. For both C_{16}GGGhex and C_{16}SGKGHhex, the optimal phosphate binding occurs at pH 6, with minimal binding occurring at low and high pH extremes. Intuitively, as the ratio of PA to phosphate increases, the amount of captured phosphate in solution also increases. C_{16}GGGhex achieved phosphate capture of 92% and 100% at pH 6 and a molar ratio of 3:1 and 5:1 PA binding unit to phosphate, respectively. Comparatively, C_{16}SGKGHhex only achieved 79% binding at identical 5:1 ratio conditions. Additionally, increasing the ratio further to 10:1 did not achieve the complete phosphate capture as exhibited by C_{16}GGGhex. The superior performance of C_{16}GGGhex places this material on par to meet the strict phosphate effluent limits, which can be as low as 0.1 mg/L of phosphorus.[10]

The kinetics experiments (see Figure S11) demonstrated that C_{16}GGGhex sequestered and released phosphate within seconds to minutes of reaching the target pH, and the material maintains its unbound or bound state as long as the pH remains constant. This rapid succession

between capture and release states eliminates any need for equilibrating binding time, an additional process design advantage. In light of these binding results, we chose to continue additional characterization only for the superiorly performing PA micelle, C_{16}GGGhex, at a ratio of 5:1 PA:PO_4 with a capture pH of 6 and two potential release pH's of 2 and 11.

The superior binding ability of C_{16}GGGhex over C_{16}SGKGHhex illuminates three interesting binding implications. First, it appears that binding is notably impacted by the entire PA molecule design, even though both designs utilize the same binding moiety. Second, binding is not maximized by increasing charged interactions. C_{16}SGKGHhex has a +6 charge at neutral pH (from 3 histidines, 2 lysines, and 1 amine N-terminus), while C_{16}GGGhex only has a charge of +1. Nevertheless, C_{16}GGGhex achieves maximal binding of the anion, presumably from superiorly employing the P-loop binding mechanism for targeted capture. Third, binding is achieved by both spherical and wormlike micelle architectures, with no notable differences in performance. C_{16}SGKGHhex transitions from spheres to worms, but the binding profile follows a comparable trend as C_{16}GGGhex.

The most notable implication, however, was that the binding properties appear to be significantly impacted by the self-assembled state of the PAs compared to unassembled hexapeptides not conjugated to a tail. Contrary to the results of our micelle material, namely maximal binding at pH 6 and minimal binding as pH increases, previous experimental studies of the free peptide observed the opposite, with highest phosphate binding at high pH and minimal binding at and below pH 6.[32] A simulation study on the same peptide, in its lysine-protonated, zwitterionic state, confirmed that binding with HPO_4^{2-} is favored over H_2PO_4.[49] Moreover, as the pH rises above the pK_a of lysine sidechain at 10.5, Bianchi et al. observed that the unprotonated lysine side chain had an important role in wrapping around the phosphate to stabilize the bound complex. These works combined indicate that both protonation states of the free hexapeptide stabilize HPO_4^{2-} by forming a nested cavity and incorporating the side chain, performing the P-loop mechanism for phosphate binding.

We hypothesize that the assembled structure induces a pH shift in the binding trigger, fundamentally altering the capture and release functionality of the peptide. This is supported by the results of our simulations. The TEM images at high pH for both PAs already alluded to an intriguing macroscopic phenomenon, namely the spontaneous bundling of wormlike micelles correlated to deprotonation of lysine, that could feasibly impact phosphate binding. We propose that while the free peptide is unconstrained and able to adopt any conformation to stabilize binding of the phosphate ion at the full pH range, the peptide in our system, which already is more constrained in the micelle, becomes even more confined as pH rises and approaches the pK_a of lysine. As the lysine charges in the headgroup are neutralized and no longer repel each other, the micelle headgroup collapses and thereby eradicates any conformational freedom that previously allowed the free peptides to sequester the phosphate ions. The collapse of micelle coronae is later quantitatively confirmed by our simulations. Therefore, although previous results show that high pH is the optimal binding state for this peptide, our self-assembled micelle system distorts the peptide binding conformation within each micelle, eliminates further conformational freedom by the micelles collapsing together upon each other, and fundamentally alters the binding ability at high pH.

Interestingly, we do not simply observe zero binding at the full pH range, as would be expected in light of the collapsed micelle morphology at high pH; instead, we see a pH shift of binding. Whereas other systems observed decreased-to-no binding below pH 6, we observe pH 6 as our maximal binding condition, with binding occurring in decreased efficacy until reaching pH 2. As our simulation results later confirm, phosphate is bound at this pH condition by the densely packed, positively charged headgroup in the micelle corona that attracts and conformationally stabilizes the negatively charged $H_2PO_4^-$ through nested hydrogen bonding. Not only is this binding pH shift induced by peptide aggregation scientifically intriguing and useful for informing future material designs, but it also has beneficial implications for resource reclamation. It is much more convenient to operate the phosphate collection conditions near the equilibrium pH of the system, which rests around neutral pH, and to perform the release conditions at the more unstable pH extremes, compared to vice versa. Overall, this system proved to capture phosphate completely and release phosphate at low and high pH values within minutes, while maintaining reversible structural stability to facilitate practical phosphate reclamation, which we were positioned to evaluate next.

2.4 Simulation Results Elucidate Binding Properties

To investigate the nanoscale mechanisms for the pH shift, we applied unbiased molecular dynamics (MD) simulations and the adaptive biasing force (ABF) enhanced sampling method [50,51] to study phosphate binding of both the unimer and self-assembled C_{16}GGGhex at pH 6 and 11. The pH states are represented by the differing protonation states of the phosphate ion and the PA lysine sidechain, with pH 6 consisting of phosphate as $H_2PO_4^-$ and a protonated lysine amine, and pH 11 consisting of phosphate as HPO_4^{2-} and a deprotonated lysine amine. We studied the unimer PA first to determine whether the molecular alterations of the PA were the cause of the pH binding shift. Then we tested the assembled micelle system to further examine how binding is impacted by a dense, assembled peptide environment.

2.4.1 Phosphate-binding to Unimer PA

Compared to the free hexapeptide with natural C and N termini, the hexapeptide in the PA is conjugated with three additional glycine residues on the N terminal and is amidated on its C terminal, which could likely disrupt binding behavior compared to that of the free peptide. To determine this, we screened the bound PA-phosphate structures using unbiased MD. For each pH condition, 9 unbiased MD trajectories with different starting configurations were collected. Snapshots were collected every 10 ps for a total of 9009 snapshots for each pH condition. The snapshots were rotationally and translationally aligned by the peptide coordinates and were subsequently analyzed using the GROningen MAchine for Chemical Simulations (GROMACS) cluster tool.[52,53] The unbiased MD information was later used to define collective variables (CVs) to describe the system dynamics, which were then used in ABF enhanced sampling simulations to study the thermodynamics of binding at each pH condition.

For each pH condition, the phosphate interacted with the PA through various mechanisms, with the top five most commonly observed clusters presented in Figure 4A. At pH 6, phosphate was found to be bound only in the third cluster and unbound in the other clusters shown. In contrast, at pH 11, the phosphate was bound by C_{16}GGGhex in all of the top five most common clusters, but the binding was stabilized at

multiple locations, some of which included the GGG spacer in addition to the hexapeptide. In regards to observing the proposed P-loop mechanism of binding, we identified several clusters at both pH's in which the phosphate was surrounded by a 3-pronged "claw" formed by the hexapeptide backbone and its lysine side chain. This is consistent with the previously studied "nested cavity" P-loop mechanism for binding. These results agree with previous characterizations in that the hexapeptide prefers to bind phosphate at high pH rather than at low pH, and indicate that the physics built into our models are consistent with past reports for single molecules.

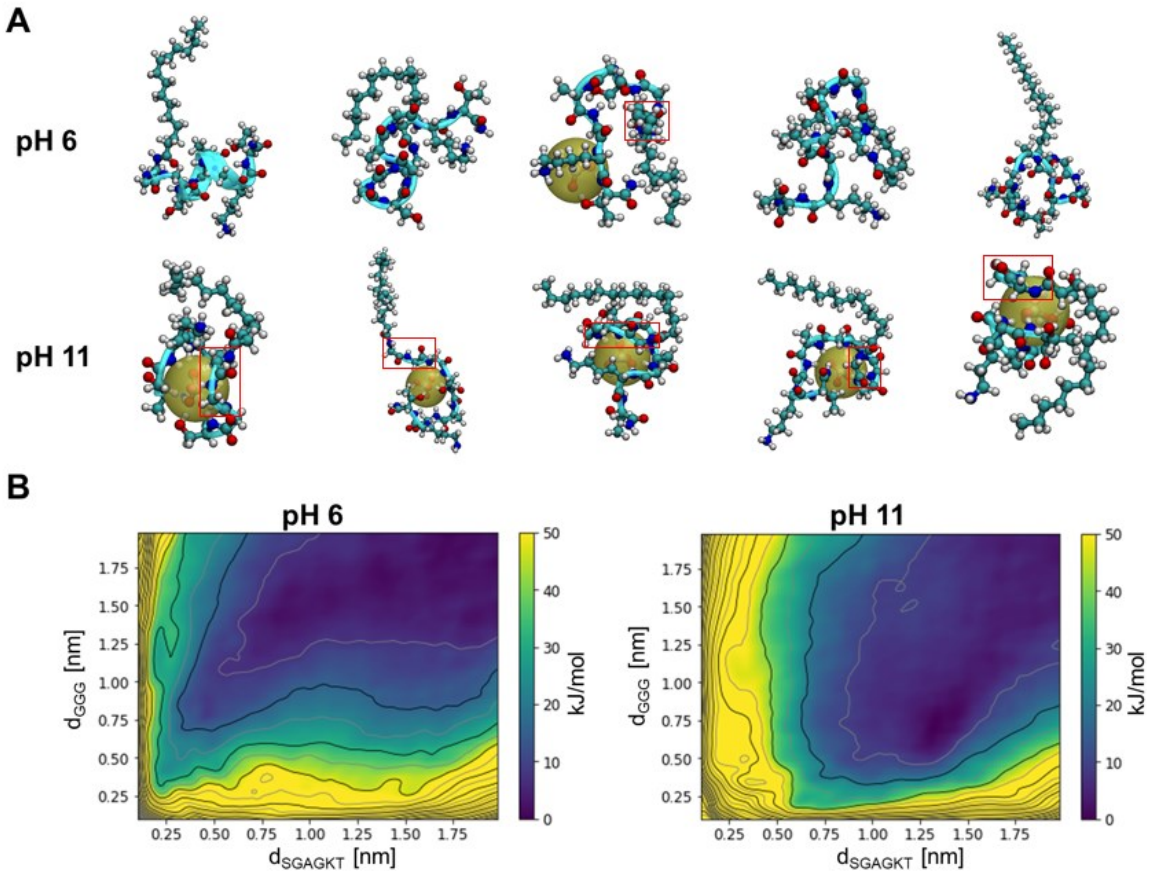

Figure 4. Single-chain binding simulations of C_{16}GGGhex show that binding is preferred at pH 11. (A) Snapshots of the top five populated clusters obtained in unbiased MD simulations. Populations of clusters decrease from left to right. The snapshots reveal the GGG spacer (boxed in red) and hexapeptide are the two major regions of phosphate binding along the PA chain. (B) Free energy surface obtained via ABF sampling for single-chain PA binding to one phosphate. At pH 6, free energy is lowest for the unbound state (upper right corner). At pH 11, a bound state at d_{SGAGKT}=1.34nm, d_{GGG}=0.74nm is preferred with a binding free energy of -2.8 kJ/mol.

These snapshots also highlight that the spacers, incorporated into the molecular design to tune the micellar architecture, are not passive participants in binding but rather play an active role in stabilizing the phosphate. To qualify this phenomenon further, we calculated free energy surfaces in terms of two distance CV's to characterize binding of the unimer PA to phosphate: (1) d_{SGAGKT}, distance from the phosphate to the center of the 3-prong SGAGKT binding pocket; and (2) d_{GGG}, distance from the phosphate to the center of the GGG binding region (additional details provided in SI). We used these two CVs to perform ABF simulations to calculate the free energy landscape of one phosphate ion binding to a unimer PA at each pH condition. The results are shown in Figure 4B.

Our simulations confirm that phosphate is unbound at pH 6 and that it binds to the unimer PA utilizing the GGG spacer in addition to the hexapeptide. For pH 6, the free energy minimum, corresponding to the most stable binding state, is located at the top right corner of the free energy surface. This location corresponds to a phosphate ion far from both binding regions of the PA, simply stable in aqueous solution, suggesting that C_{16}GGGhex fails to sequester phosphate at pH 6. At pH 11, however, a minimum is found at d_{SGAGKT}=1.34, d_{GGG}=0.74 with a free energy difference of -2.8 kJ/mol with respect to the unbound state. This free energy minimum occurs at low d_{GGG} values, suggesting that interaction with the GGG linker is important for phosphate binding to the PA at pH 11. The free energy results confirm the finding that, unlike phosphate-binding to the SGAGKT hexapeptide, phosphate-binding to this PA exhibits more flexible binding structures, where the bound phosphate can interact with both the spacer and hexapeptide regions.

2.4.2 Phosphate-binding to Peptide Amphiphile Micelle

Having verified that the molecular alterations did not shift the pH binding conditions of the unimer PA, we simulated a micelle system to probe how the densely packed self-assembled environment impacts binding. We used unbiased MD simulations to characterize the phosphate binding behaviors of the micelle at an approximate PA:PO_4 ratio of 5:1. For each pH condition, 40 phosphate and 216 PA chains were simulated in water. Sodium (Na^+) or chloride (Cl^-) ions were added to neutralize the simulation box. The last 20-ns of the 50-ns MD trajectory under an

isothermal-isobaric ensemble were used for analysis (details in SI). The simulated micelle was periodic along its cylindrical axis, which is aligned in the z-direction.

Our micelle simulations confirm the experimental shift in binding pH that is induced when the PA molecules systematically self-assemble. We corroborated this simulated binding shift using three complementary approaches: a histogram analysis of the radial distance of the phosphate to the micelle core, a potential of mean force (PMF) estimation, and a hydrogen bond (H-bond) analysis. Visually, we observe in Figure 5A two top-down snapshots of the simulated system, depicting the majority of phosphate ions being bound at pH 6, while most phosphate ions were unbound at pH 11. The visual analysis was further corroborated using a histogram of the radial distance of the phosphate ions to the micelle core (Figure 5B). These distances were then compared to the distance to the possible PA binding sites that were observed in the single-molecule PA analysis, namely the hexapeptide and the GGG spacer. Indeed, at pH 11, the distance of the phosphate to the center of the micelle was not localized anywhere, signifying an unbound state. But for pH 6, the majority of phosphate ions were located at the same distance from the core as the hexapeptide sequence, confirming localized binding to the hexapeptide.

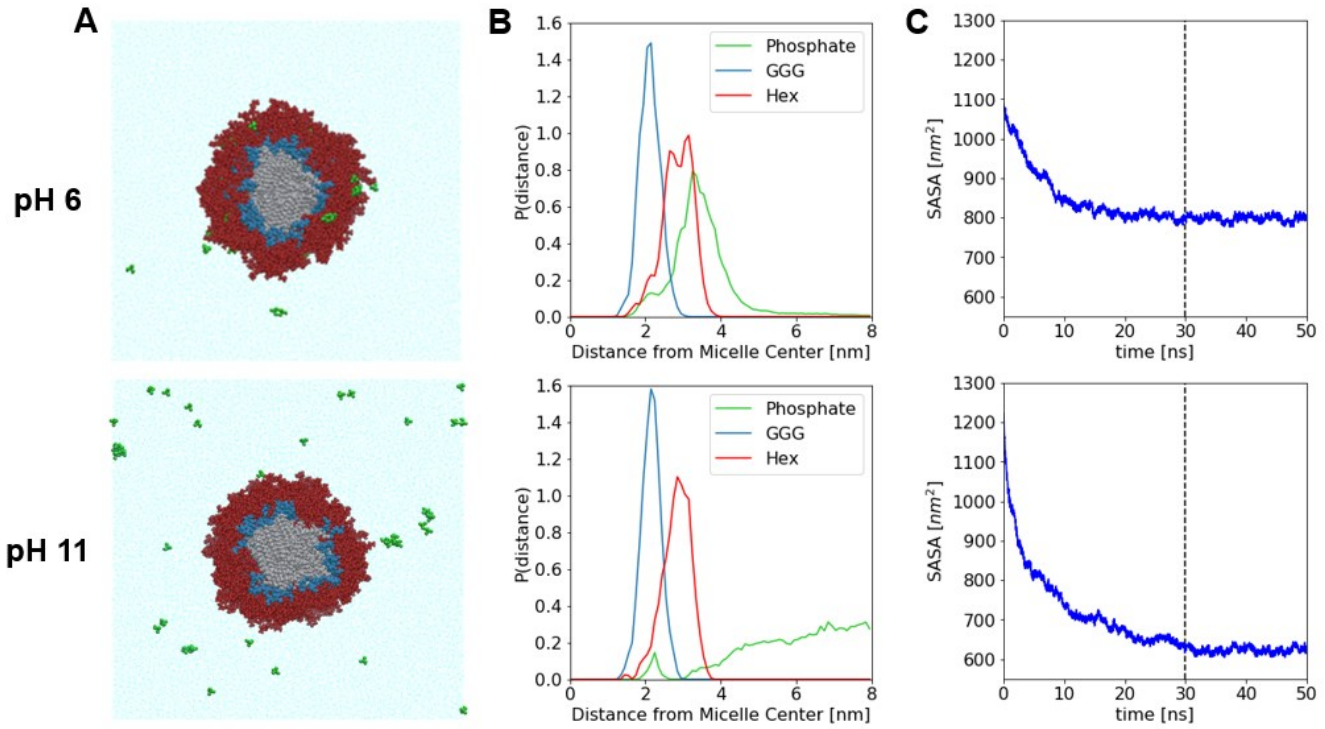

Figure 5. Simulations of phosphate binding to the C_{16}GGGhex micelle at pH 6 and 11. (A) Top-down snapshots of the simulated micelles at the end of the production run. (B) Normalized histograms of radial position from the micelle central axis for different components in the systems. The GGG spacer is noted as 'GGG' and the SGAGKT hexapeptide as 'Hex' in the legend. (C) Solvent-accessible surface area (SASA) of the micelle as a function of simulation time. The dash lines indicate the start of the time-averaging interval. The average SASA values are 798 ± 9 $nm^2$and 623 ± 8 nm^2 at pH 6 and 11, respectively.

The potential of mean force (PMF) offers insight into the free energy of binding of phosphate to the micelle compared to the unimer PA, with a lower free energy signifying a more stabilized bound state. The PMF along the radial CV was estimated by computing the Boltzmann inversion on the corresponding probability distribution via the equation $PMF(r) = kTln(P(r))$, where k is the Boltzmann constant and T is the temperature. Here, the PMF was computed as a function of distance from the micelle center, and $P(r)$ is the normalized histogram of the radial position of phosphate ions. From the PMF results (Figure S14), we estimated that the PMF for a phosphate to bind to the micelle at pH 6 was -11.7 kJ/mol, which is lower by a factor of four than the binding free energy for phosphate binding to a single PA at pH 11 (-2.8 kJ/mol). Interestingly, this result highlights that binding at pH 6 in the assembled state is even more stabilized compared to binding to the unimer PA at pH 11.

Finally, an H-bond analysis was performed to quantify the binding percentage of phosphate to the micelle at both pH states. We define the binding percentage to be the percent of time that a phosphate forms at least one H-bond with the micelle, averaged over the simulation time and phosphate samples. This was found to be 59% and 0.4% at pH 6 and 11, respectively. Though the simulated binding percentage at pH 6 is lower than the experimental measurement of complete capture, these values qualitatively capture the significant difference between binding performances at pH 6 and 11.

Having quantified that the pH shift is in fact occurring, we probed the fundamental reason for why. For pH 11, we noted two phenomena that caused this decrease in binding, one pertaining to a per-molecule analysis and the other pertaining to a newly emergent and noteworthy bulk property. The per-molecule insight was derived from the radial histogram data. When binding did occur at pH 6 (Figure 5B), we observed that GGG no longer interacted with the phosphate in the assembled state, even though previously GGG played an active role in stabilizing phosphate as a unimer PA, especially for pH 11. It is likely that the densely packed corona prohibited the phosphate from penetrating deep

enough into the corona to fully utilize the additional hydrogen bonds of the GGG backbone. With these key components of binding now inaccessible in the micelle state, phosphate was unable to be bound and stabilized at high pH.

Second, we were motivated by the TEM images of clustered PA micelles (Figure 2C) to probe how the lysine side chain deprotonation influences binding according to a bulk micellar mechanism. As discussed previously, the micelle was apparently teetering on the edge of insolubility, so simply approaching the pK_a and deprotonating a small fraction of lysine amines causes to micelles to clump together. To quantify the impact of this phenomenon on binding, we relied on the solvent-accessible surface area (SASA) for the entire micelle to measure the extent of headgroup presentation to the aqueous environment, and thereby to the phosphate ions. Using the GROMACS SASA tool,[54] the time-averaged SASA was found to be 798 ± 9 and 623 ± 8 nm^2 at pH 6 and 11, respectively. These results suggest that the deprotonation of lysine leads to a statistically significant decrease in micellar surface area, and with that a decrease in access to binding sites. Thus, as more of the lysine amines become deprotonated, the micelle corona gradually collapses and expels more and more phosphate, corresponding to the decreased binding in Figure 3A as pH rises. The simulated system of all deprotonated lysine amines shows this to the extreme, when the micelle is fully collapsed and phosphate is completely expelled or "squeezed" out of the micelle. Thus, compared to a unimer PA, under assembled conditions, phosphate is no longer able to penetrate the even denser micellar headgroup, and binding becomes impossible, explaining the first part of the pH shift.

To understand the increase in binding stability at pH 6, we utilized data from the H-bonding analysis. In the assembled system, we observed multiple chains involved in binding to stabilize the phosphate in the headgroup in the densely packed corona (Figure S15). The multi-chain binding behavior is a direct result of the PA micelle assembly, where multiple binding opportunities are simultaneously presented to the phosphate ions. This result is also corroborated by our ratio of PA:PO_4 experiments (Figure 3C), which elucidated that multiple chains per phosphate were necessary to achieve complete bulk phosphate capture. This binding mechanism is not available for a single peptide, nor has it been previously remarked on in single-chain binding studies, presenting an additional advantage of this self-assembled binding system where increased binding stability is introduced.

2.5 Selectivity Over Nitrate and Nitrite

With knowledge of the fundamental binding properties, we experimentally evaluated the selectivity of C_{16}GGGhex to bind to phosphate in the presence of competing oxyanions, probing the molecular recognition of this material. We chose nitrate and nitrite as the competing anions since those would be the primary competitors in agricultural runoff streams that are rich in these three fertilizer components.[10] In our experiments, we introduced equimolar amounts of nitrate, nitrite, and phosphate to systems with 1x, 2x, and 3x molar excess of C_{16}GGGhex at pH 6, equivalent to 10 ppm phosphate. The results are shown in Figure 6.

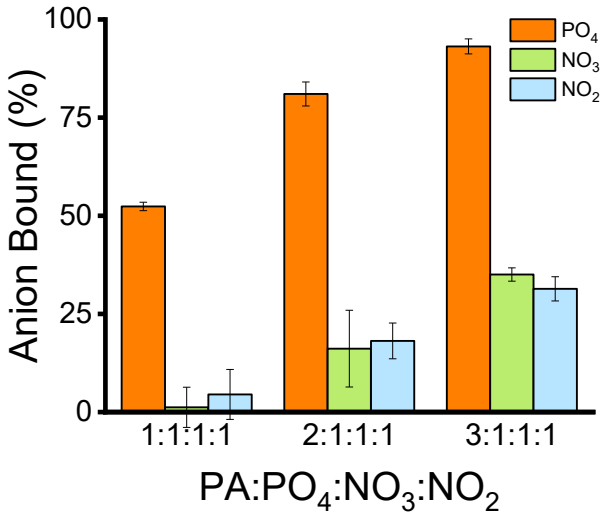

Figure 6. Selectivity results for C_{16}GGGhex at pH 6 with molar ratios equivalent to 10 ppm phosphate. Phosphate is bound more than nitrate and nitrite in all cases. In the case of equimolar PA to phosphate, C_{16}GGGhex binds 52% of the phosphate present and less than 5% of nitrate and nitrite, exhibiting excellent selectivity in these conditions. As the concentration of PA increases, C_{16}GGGhex begins to bind to nitrite and nitrate in a linearly increasing trend, while still binding phosphate most.

In all cases, we observe that C_{16}GGGhex binds to phosphate significantly more than to either of the competing oxyanions. In the 1:1:1:1 case, C_{16}GGGhex binds less than 5% of nitrate and nitrite but is still able to sequester 52% of phosphate, consistent with its binding performance without competing ions (see Figure 3C). Thus, at this lower concentration of PA, we observe excellent selectivity and see C_{16}GGGhex performing its designed-in molecular recognition functionality. As we increase the amount of PA in the system, C_{16}GGGhex continues to bind phosphate aligned with the previously observed amounts in Figure 3C, but it discriminates phosphate less, following a linear trend of binding increasing amounts of nitrate and nitrite up to 35% and 31%, respectively. This trend could be indicative of the molecular-recognition P-loop being less exclusively employed to capture phosphate through the signature selective nested cavity formation. Instead, C_{16}GGGhex is likely indiscriminately binding nitrite and nitrate by electrostatic attraction to the positively charged lysine, whose abundance increases as the PA concentration increases. It could also be that the densely packed corona prohibits the peptides from adopting the molecular-recognition P-loop nested cavity formation as readily, decreasing its designed-in means to select only phosphate. However, because we do not simply observe

proportionate binding of anions in each case but rather observe a linear binding trend that ends in nearly zero binding of competitors, a strong case can be made for P-loop molecular recognition in the 1:1:1:1 conditions.

While these preliminary results present opportunities for optimizing exclusive binding to phosphate even with excess binding sites present, we nonetheless observe molecular preference for phosphate in all cases, with particular success in discriminating between phosphate and its competitors with equimolar amounts of binding sites and phosphate. To harken back to our previous findings in considering routes for optimization, the unique multi-chain binding observed in our micelle simulations presents an intriguing starting point, specific to the versatility PA micelles, to design increased molecular selectivity in future rounds of synthesis.

2.6 Cycles of Capture and Release

Finally, we evaluated the capture, release, and reclamation functionality of this material, as well as its durability upon cycles of reuse, providing valuable information for the practical phosphate reclamation potential of our material platform. We sequentially adjusted the pH from 6 to the acidic or basic release pH, collecting and analyzing the filtrate at each step. After filtration at the release pH, we added phosphate to re-achieve a starting concentration of 50 ppm, as calculated from the phosphate concentration of the filtrate.

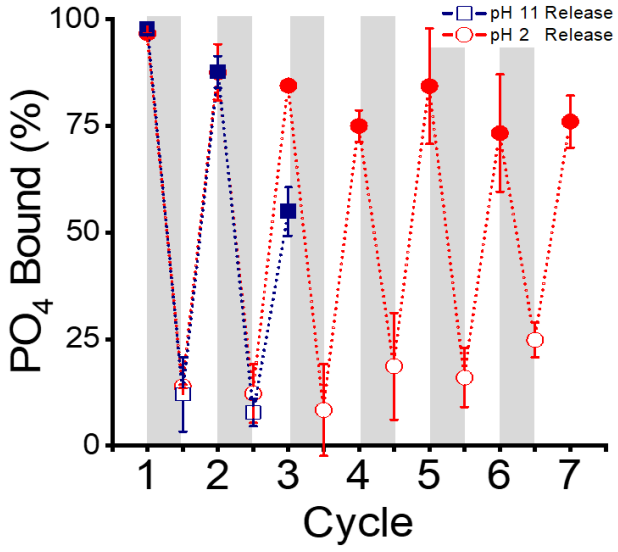

Figure 7. Capture and release results for C_{16}GGGhex. The filled-in markers represent the pH 6 capture condition, while the open markers represent the release condition of either pH 2 or 11. The gray rectangle depict the release step from pH 6 to either pH 2 or 11. The material demonstrates an ability to reversibly capture and release phosphate for both the release pH 2 and pH 11. For the pH 11 release condition, the material becomes unable to rebind nearly half of the present phosphate after 3 cycles. It was noted that the solution turns notably cloudy, highlighting how the PA aggregation at high pH likely contributed to a decreased ability to rebind phosphate. For the pH 2 release condition, the material could rebind greater than 73% of phosphate and release up to 75% of phosphate for up to 7 cycles, becoming the superior release condition.

The cycles of capture and release data in Figure 7 demonstrate that our material does indeed perform sequential binding and release, and it also highlighted interesting material properties at pH 11. For pH 2 triggered release, the material was able to expel and rebind phosphate for up to the 7 cycles tested, rebinding up to 73% each time and releasing up to 75%. The capture and release performance both diminish as the number of cycles increases, which could be a function of increased time required to achieve equilibrium after successive cycles, highlighting the potential for optimization of this process. The material using a pH 11 triggered release, on the other hand, exhibited a sharp decrease in ability to rebind after only 3 cycles, binding only 55% of the added phosphate in solution. Since this performance was markedly worse, we ceased performing further cycles under this release condition after this point. We believe that this trend is occurring due to the clumping of micelles observed at high pH, which was visually supported by a significant increase in cloudiness of the sample after successive cycles. Thus, it appears that the fundamentally altered binding ability at pH 11, as observed in the simulation results, also negatively impacts the functionality of the material when operating repetitively at these basic release conditions. The decrease in binding for both systems could also be due to loss of unimer PAs upon wash steps. This loss could be averted by locking the assemblies through internal covalent crosslinks, a straightforward design change that has been employed previously,[23] which could increase the robustness and recyclability of the PA micelle network.

In sum, these data demonstrate that our material is capable of successive capture and release of phosphate, as opposed to remaining permanently bound like many adsorbents,[55–57] with promise for further process optimization. More broadly, they highlight the feasibility of using an entangled wormlike micelle structure with phosphate binding units coating the fibers to practically catch, retain, and separate out the phosphate from water, an advantage over the free-floating peptides which would be difficult to partition out from the solution.

3. Conclusion

We have designed, synthesized, and characterized a prototype of a materials platform to capture and reclaim phosphate, utilizing self-assembled peptide amphiphiles that easily incorporate specific protein-inspired binding sequences to molecularly recognize their specific targets. These peptide amphiphile wormlike micelles form a dense entangled suspension that becomes a solid support for straightforward collection of phosphate in response to a pH trigger. The PA material C_{16}GGGhex sequestered 100% of phosphate at pH 6 and released up to

75% at pH 2 for up to seven cycles. C_{16}GGGhex also was found to selectively bind to phosphate over nitrate and nitrite. Detailed atomistic simulations with advanced sampling confirm that the assembled state of the material fundamentally alters the pH binding functionality compared to the free peptide, shifting the maximal binding conditions from pH 10.5 to 6 due to the micellar headgroup becoming conformationally constrained at high pH, thereby expelling the phosphate. At pH 6, simulations indicate that unimer PAs do not bind phosphate, but they are able to do so via multi-chain binding when assembled into a micelle. Our simulations serve to highlight the important role of PA packing in phosphate binding behavior and suggest a new multi-chain phosphate-binding mechanism that is unique to PA micelles, reminiscent of the tertiary structure adopted by proteins for targeted binding. These findings indicate that PA packing in micelles is an important design factor, thus opening up a new avenue of relying upon multi-chain binding motifs for the design of selective ion-sequestering materials.

This work represents a first step in our aim to incorporate protein-inspired design into a tunable synthetic material for practical resource reclamation from wastewater. Since this material platform so naturally incorporates protein-inspired binding sequences, we are positioned to easily modify the binding sequence to target a wide array of other valuable resources in wastewater. Overall, if proven to be scalable and cost-effective, this novel materials platform could potentially provide a paradigm shift in materials development for specific capture and reclamation for wastewater.

ASSOCIATED CONTENT

Supporting Information

The Supporting Information is available free of charge on the ACS Publications website.

Methods, author contributions, and additional data including MALDI-TOF, kinetics experiments, CMC, TEM, molybdenum blue reaction assay, effect of NaCl on binding, and simulation results (PDF)

AUTHOR INFORMATION

Corresponding Authors

* Matthew V. Tirrell – mtirrell@uchicago.edu
* Juan J. de Pablo – depablo@uchicago.edu
* Moshe Gottlieb – mosheg@bgu.ac.il

ACKNOWLEDGMENT

This work was supported by the National Science Foundation DMR-1710357, the U.S. Israel Binational Science Foundation Grant 2016664, and the NSF-BSF Grant 2016664. W.C.F. acknowledges support from the National Science Foundation (NSF) Graduate Research Fellowship Program under Grant No. (DGE-1746045). M.Z. acknowledges support from the Kreitman Post-doctoral Research Fellowship. The authors would like to acknowledge the University of Chicago's Advanced Electron Microscopy Core Facility for acquiring the TEM images, as well as the University of Chicago's Mass Spectroscopy Core Facility, where LC-MS and MALDI-TOF data were acquired. Analyte analysis by ion chromatography was performed at the Northwestern University Quantitative Bio-element Imaging Center. The simulations were completed on computational resources provided by the University of Chicago Research Computing Center. The authors also thank Amanda B. Marciel for an important role in the conception of this project, Jihyeon Yeo for pH binding data collection and helpful discussions, and Jeffrey M. Ting for helpful discussions.

REFERENCES

(1) Grant, S. B.; Saphores, J.-D.; Feldman, D. L.; Hamilton, A. J.; Fletcher, T. D.; Cook, P. L. M.; Stewardson, M.; Sanders, B. F.; Levin, L. A.; Ambrose, R. F.; et al. Taking the "Waste" Out of "Wastewater" for Human Water Security and Ecosystem Sustainability. *Science.* **2012**, *337* (6095), 681–686. https://doi.org/10.1126/science.1216852.

(2) WWAP (United Nations World Water Assessment Programme). *The United Nations World Water Development Report 2017. Wastewater: The Untapped Resource*; UNESCO: Paris, 2017.

(3) Van Loosdrecht, M. C. M.; Brdjanovic, D. Anticipating the Next Century of Wastewater Treatment. *Science.* **2014**, *344* (6191), 1452–1453. https://doi.org/10.1126/science.1255183.

(4) Mo, W.; Zhang, Q. Energy-Nutrients-Water Nexus: Integrated Resource Recovery in Municipal Wastewater Treatment Plants. *J. Environ. Manage.* **2013**, *127*, 255–267. https://doi.org/10.1016/j.jenvman.2013.05.007.

(5) Liu, C.; Hsu, P. C.; Xie, J.; Zhao, J.; Wu, T.; Wang, H.; Liu, W.; Zhang, J.; Chu, S.; Cui, Y. A Half-Wave Rectified Alternating Current Electrochemical Method for Uranium Extraction from Seawater. *Nat. Energy* **2017**, *2* (4), 1–8. https://doi.org/10.1038/nenergy.2017.7.

(6) De-Bashan, L. E.; Bashan, Y. Recent Advances in Removing Phosphorus from Wastewater and Its Future Use as Fertilizer (1997-2003). *Water Res.* **2004**, *38* (19), 4222–4246. https://doi.org/10.1016/j.watres.2004.07.014.

(7) Kolpin, D. W.; Furlong, E. T.; Meyer, M. T.; Thurman, E. M.; Zaugg, S. D.; Barber, L. B.; Buxton, H. T. Pharmaceuticals, Hormones, and Other Organic Wastewater Contaminants in U.S. Streams, 1999-2000: A National Reconnaissance. *Environ. Sci. Technol.* **2002**, *36* (6), 1202–1211. https://doi.org/10.1021/es011055j.

(8) Gros, M.; Petrović, M.; Ginebreda, A.; Barceló, D. Removal of Pharmaceuticals during Wastewater Treatment and Environmental Risk Assessment Using Hazard Indexes. *Environ. Int.* **2010**, *36* (1), 15–26. https://doi.org/10.1016/j.envint.2009.09.002.

(9) Puyol, D.; Batstone, D. J.; Hülsen, T.; Astals, S.; Peces, M.; Krömer, J. O. Resource Recovery from Wastewater by Biological Technologies: Opportunities, Challenges, and Prospects. *Front. Microbiol.* **2017**, *7*, 1–23. https://doi.org/10.3389/fmicb.2016.02106.

(10) Mehta, C. M.; Khunjar, W. O.; Nguyen, V.; Tait, S.; Batstone, D. J. Technologies to Recover Nutrients from Waste Streams: A Critical Review. *Crit. Rev. Environ. Sci. Technol.* **2015**, *45* (4), 385–427. https://doi.org/10.1080/10643389.2013.866621.

(11) Cai, T.; Park, S. Y.; Li, Y. Nutrient Recovery from Wastewater Streams by Microalgae: Status and Prospects. *Renew. Sustain. Energy Rev.* **2013**, *19*, 360–369. https://doi.org/10.1016/j.rser.2012.11.030.

(12) Yuan, Z.; Pratt, S.; Batstone, D. J. Phosphorus Recovery from Wastewater through Microbial Processes. *Curr. Opin. Biotechnol.* **2012**, *23* (6), 878–883. https://doi.org/10.1016/j.copbio.2012.08.001.

(13) Le Corre, K. S.; Valsami-Jones, E.; Hobbs, P.; Parsons, S. A. Phosphorus Recovery from Wastewater by Struvite Crystallisation: A Review. *Crit. Rev. Environ. Sci. Technol.* **2009**, *39* (6), 433–477. https://doi.org/10.1017/CBO9781107415324.004.

(14) Lee, C.-G.; Alvarez, P. J. J.; Kim, H.-G.; Jeong, S.; Lee, S.; Lee, K. B.; Lee, S.-H.; Choi, J.-W. Phosphorous Recovery from Sewage Sludge Using Calcium Silicate Hydrates. *Chemosphere* **2018**, *193*, 1087–1093. https://doi.org/10.1016/j.chemosphere.2017.11.129.
(15) Cordell, D.; Rosemarin, A.; Schröder, J. J.; Smit, A. L. Towards Global Phosphorus Security: A Systems Framework for Phosphorus Recovery and Reuse Options. *Chemosphere* **2011**, *84* (6), 747–758. https://doi.org/10.1016/j.chemosphere.2011.02.032.
(16) Harris, S. M.; Nguyen, J. T.; Pailloux, S. L.; Mansergh, J. P.; Dresel, M. J.; Swanholm, T. B.; Gao, T.; Pierre, V. C. Gadolinium Complex for the Catch and Release of Phosphate from Water. *Environ. Sci. Technol.* **2017**, *51* (8), 4549–4558. https://doi.org/10.1021/acs.est.6b05815.
(17) Su, Z.; Hostert, J. D.; Renner, J. N. Phosphate Recovery by a Surface-Immobilized Cerium Affinity Peptide. *ACS ES&T Water* **2020**, *1* (1). https://doi.org/10.1021/acsestwater.0c00001.
(18) Desmidt, E.; Ghyselbrecht, K.; Zhang, Y.; Pinoy, L.; Van Der Bruggen, B.; Verstraete, W.; Rabaey, K.; Meesschaert, B. Global Phosphorus Scarcity and Full-Scale P-Recovery Techniques: A Review. *Crit. Rev. Environ. Sci. Technol.* **2015**, *45* (4), 336–384. https://doi.org/10.1080/10643389.2013.866531.
(19) Cisse, L.; Mrabet, T. World Phosphate Production: Overview and Prospects. *Phosphorus Res. Bull.* **2004**, *15*, 21–25.
(20) Cordell, D.; Drangert, J. O.; White, S. The Story of Phosphorus: Global Food Security and Food for Thought. *Glob. Environ. Chang.* **2009**, *19* (2), 292–305. https://doi.org/10.1016/j.gloenvcha.2008.10.009.
(21) Smith, V. H.; Schindler, D. W. Eutrophication Science: Where Do We Go from Here? *Trends Ecol. Evol.* **2009**, *24* (4), 201–207. https://doi.org/10.1016/j.tree.2008.11.009.
(22) Zhu, H.; Wang, H.; Shi, B.; Shangguan, L.; Tong, W.; Yu, G.; Mao, Z.; Huang, F. Supramolecular Peptide Constructed by Molecular Lego Allowing Programmable Self-Assembly for Photodynamic Therapy. *Nat. Commun.* **2019**, *10* (1), 1–10. https://doi.org/10.1038/s41467-019-10385-9.
(23) Hartgerink, J. D.; Beniash, E.; Stupp, S. I. Self-Assembly and Mineralization of Peptide-Amphiphile Nanofibers. *Science.* **2001**, *294* (5547), 1684–1688.
(24) Trent, A.; Marullo, R.; Lin, B.; Black, M.; Tirrell, M. Structural Properties of Soluble Peptide Amphiphile Micelles. *Soft Matter* **2011**, *7* (20), 9572–9582. https://doi.org/10.1039/c1sm05862b.
(25) Missirlis, D.; Chworos, A.; Fu, C. J.; Khant, H. A.; Krogstad, D. V.; Tirrell, M. Effect of the Peptide Secondary Structure on the Peptide Amphiphile Supramolecular Structure and Interactions. *Langmuir* **2011**, *27* (10), 6163–6170. https://doi.org/10.1021/la200800e.
(26) Peters, D.; Kastantin, M.; Kotamraju, V. R.; Karmali, P. P.; Gujraty, K.; Tirrell, M.; Ruoslahti, E. Targeting Atherosclerosis by Using Modular, Multifunctional Micelles. *Proc. Natl. Acad. Sci. U. S. A.* **2009**, *106* (24), 9815–9819. https://doi.org/10.1073/pnas.0903369106.
(27) Chung, E. J.; Cheng, Y.; Morshed, R.; Nord, K.; Han, Y.; Wegscheid, M. L.; Auffinger, B.; Wainwright, D. A.; Lesniak, M. S.; Tirrell, M. V. Fibrin-Binding, Peptide Amphiphile Micelles for Targeting Glioblastoma. *Biomaterials* **2014**, *35* (4), 1249–1256. https://doi.org/10.1016/j.biomaterials.2013.10.064.
(28) Ananthanarayanan, B.; Little, L.; Schaffer, D. V.; Healy, K. E.; Tirrell, M. Neural Stem Cell Adhesion and Proliferation on Phospholipid Bilayers Functionalized with RGD Peptides. *Biomaterials* **2010**, *31* (33), 8706–8715. https://doi.org/10.1016/j.biomaterials.2010.07.104.
(29) Li, Y.; Lock, L. L.; Mills, J.; Ou, B. S.; Morrow, M.; Stern, D.; Wang, H.; Anderson, C. F.; Xu, X.; Ghose, S.; et al. Selective Capture and Recovery of Monoclonal Antibodies by Self-Assembling Supramolecular Polymers of High Affinity for Protein Binding. *Nano Lett.* **2020**, *20* (10), 6957–6965. https://doi.org/10.1021/acs.nanolett.0c01297.
(30) Yang, Q.; Zhu, Y.; Luo, B.; Lan, F.; Wu, Y.; Gu, Z. pH-Responsive Magnetic Metal-Organic Framework Nanocomposites for Selective Capture and Release of Glycoproteins. *Nanoscale* **2017**, *9* (2), 527–532. https://doi.org/10.1039/c6nr08071e.
(31) Chen, Y.; Li, P.; Modica, J. A.; Drout, R. J.; Farha, O. K. Acid-Resistant Mesoporous Metal-Organic Framework toward Oral Insulin Delivery: Protein Encapsulation, Protection, and Release. *J. Am. Chem. Soc.* **2018**, *140* (17), 5678–5681. https://doi.org/10.1021/jacs.8b02089.
(32) Hasan, Z.; Jhung, S. H. Removal of Hazardous Organics from Water Using Metal-Organic Frameworks (MOFs): Plausible Mechanisms for Selective Adsorptions. *J. Hazard. Mater.* **2015**, *283*, 329–339. https://doi.org/10.1016/j.jhazmat.2014.09.046.
(33) Tu, R. S.; Tirrell, M. Bottom-up Design of Biomimetic Assemblies. *Adv. Drug Deliv. Rev.* **2004**, *56* (11), 1537–1563. https://doi.org/10.1016/J.ADDR.2003.10.047.
(34) Thayer, A. M. Making Peptides At Large Scale. *Chem. Eng. News Arch.* **2011**, *89* (22), 21–25. https://doi.org/10.1021/cen-v089n022.p021.
(35) Gruber, M.; Greisen, P.; Junker, C. M.; Hélix-Nielsen, C. Phosphorus Binding Sites in Proteins: Structural Preorganization and Coordination. *J. Phys. Chem. B* **2014**, *118* (5), 1207–1215. https://doi.org/10.1021/jp408689x.
(36) Romero Romero, M. L.; Yang, F.; Lin, Y. R.; Toth-Petroczy, A.; Berezovsky, I. N.; Goncearenco, A.; Yang, W.; Wellner, A.; Kumar-Deshmukh, F.; Sharon, M.; et al. Simple yet Functional Phosphate-Loop Proteins. *Proc. Natl. Acad. Sci. U. S. A.* **2018**, *115* (51), E11943–E11950. https://doi.org/10.1073/pnas.1812400115.
(37) Saraste, M.; Sibbald, P. R.; Wittinghofer, A. The P-Loop - a Common Motif in ATP- and GTP-Binding Proteins. *Trends Biochem. Sci.* **1990**, *15* (11), 430–434. https://doi.org/10.1016/0968-0004(90)90281-F.
(38) Bianchi, A.; Giorgi, C.; Ruzza, P.; Toniolo, C.; Milner-White, E. J. A Synthetic Hexapeptide Designed to Resemble a Proteinaceous P-Loop Nest Is Shown to Bind Inorganic Phosphate. *Proteins Struct. Funct. Bioinforma.* **2012**, *80* (5), 1418–1424. https://doi.org/10.1002/prot.24038.
(39) Zhai, H.; Qin, L.; Zhang, W.; Putnis, C. V.; Wang, L. Dynamics and Molecular Mechanism of Phosphate Binding to a Biomimetic Hexapeptide. *Environ. Sci. Technol.* **2018**, *52* (18), 10472–10479. https://doi.org/10.1021/acs.est.8b03062.
(40) Lin, B. F.; Megley, K. A.; Viswanathan, N.; Krogstad, D. V.; Drews, L. B.; Kade, M. J.; Qian, Y.; Tirrell, M. V. pH-Responsive Branched Peptide Amphiphile Hydrogel Designed for Applications in Regenerative Medicine with Potential as Injectable Tissue Scaffolds. *J. Mater. Chem.* **2012**, *22* (37), 19447. https://doi.org/10.1039/c2jm31745a.
(41) Paramonov, S. E.; Jun, H. W.; Hartgerink, J. D. Self-Assembly of Peptide-Amphiphile Nanofibers: The Roles of Hydrogen Bonding and Amphiphilic Packing. *J. Am. Chem. Soc.* **2006**, *128* (22), 7291–7298. https://doi.org/10.1021/ja060573x.
(42) Israelachvili, J. N.; Mitchell, D. J.; Ninham, B. W. Theory of Self-Assembly of Hydrocarbon Amphiphiles into Micelles and Bilayers. *J. Chem. Soc. Faraday Trans. 2* **1976**, *72*, 1525. https://doi.org/10.1039/f29767201525.
(43) Schneider, C. A.; Rasband, W. S.; Eliceiri, K. W. NIH Image to ImageJ: 25 Years of Image Analysis. *Nat. Methods* **2012**, *9* (7), 671–675. https://doi.org/10.1038/nmeth.2089.
(44) Ghosh, A.; Haverick, M.; Stump, K.; Yang, X.; Tweedle, M. F.; Goldberger, J. E. Fine-Tuning the pH Trigger of Self-Assembly. *J. Am. Chem. Soc.* **2012**, *134* (8), 3647–3650. https://doi.org/10.1021/ja211113n.
(45) Gebhardt, K. E.; Ahn, S.; Venkatachalam, G.; Savin, D. A. Rod-Sphere Transition in Polybutadiene-Poly(L-Lysine) Block Copolymer Assemblies. *Langmuir* **2007**, *23* (5), 2851–2856. https://doi.org/10.1021/la062939p.
(46) Nagul, E. A.; McKelvie, I. D.; Worsfold, P.; Kolev, S. D. The Molybdenum Blue Reaction for the Determination of Orthophosphate Revisited: Opening the Black Box. *Anal. Chim. Acta* **2015**, *890*, 60–82. https://doi.org/10.1016/j.aca.2015.07.030.
(47) Ganesh, S.; Khan, F.; Ahmed, M. K.; Velavendan, P.; Pandey, N. K.; Kamachi Mudali, U. Spectrophotometric Determination of Trace Amounts of Phosphate in Water and Soil. *Water Sci. Technol.* **2012**, *66* (12), 2653. https://doi.org/10.2166/wst.2012.468.
(48) Bunce, J. T.; Ndam, E.; Ofiteru, I. D.; Moore, A.; Graham, D. W. A Review of Phosphorus Removal Technologies and Their Applicability to Small-Scale Domestic Wastewater Treatment Systems. *Front. Environ. Sci.* **2018**, *6*, 1–15. https://doi.org/10.3389/fenvs.2018.00008.
(49) Gruber, M. F.; Wood, E.; Truelsen, S.; Østergaard, T.; Hélix-Nielsen, C. Computational Design of Biomimetic Phosphate Scavengers. *Environ. Sci. Technol.* **2015**, *49* (16), 9469–9478. https://doi.org/10.1021/es506214c.
(50) Comer, J.; Gumbart, J. C.; Hénin, J.; Lelievre, T.; Pohorille, A.; Chipot, C. The Adaptive Biasing Force Method: Everything You Always Wanted to Know but Were Afraid to Ask. *J. Phys. Chem. B* **2015**, *119* (3), 1129–1151. https://doi.org/10.1021/jp506633n.

(51) Sidky, H.; Colón, Y. J.; Helfferich, J.; Sikora, B. J.; Bezik, C.; Chu, W.; Giberti, F.; Guo, A. Z.; Jiang, X.; Lequieu, J.; et al. SSAGES: Software Suite for Advanced General Ensemble Simulations. *J. Chem. Phys.* **2018**, *148* (4). https://doi.org/10.1063/1.5008853.
(52) Abraham, M. J.; Murtola, T.; Schulz, R.; Páll, S.; Smith, J. C.; Hess, B.; Lindah, E. Gromacs: High Performance Molecular Simulations through Multi-Level Parallelism from Laptops to Supercomputers. *SoftwareX* **2015**, *1–2*, 19–25. https://doi.org/10.1016/j.softx.2015.06.001.
(53) Daura, X.; Gademann, K.; Jaun, B.; Seebach, D.; van Gunsteren, W. F.; Mark, A. E. Peptide Folding: When Simulation Meets Experiment. *Angew. Chemie Int. Ed.* **1999**, *38* (1/2), 236–240. https://doi.org/10.1002/(sici)1521-3773(19990115)38:1/2<236::aid-anie236>3.3.co;2-d.
(54) Eisenhaber, F.; Lijnzaad, P.; Argos, P.; Sander, C.; Scharf, M. The Double Cubic Lattice Method: Efficient Approaches to Numerical Integration of Surface Area and Volume and to Dot Surface Contouring of Molecular Assemblies. *J. Comput. Chem.* **1995**, *16* (3), 273–284. https://doi.org/10.1002/jcc.540160303.
(55) Chouyyok, W.; Wiacek, R. J.; Fryxell, G. E. Phosphate Removal by Anion Binding on Functionalized Nanoporous Sorbents. *Environ. Sci. Technol.* **2010**, *44* (8), 3073–3078. https://doi.org/https://doi.org/10.1021/es100787m.
(56) Liu, H.; Sun, X.; Yin, C.; Hu, C. Removal of Phosphate by Mesoporous ZrO2. *J. Hazard. Mater.* **2008**, *151* (2–3), 616–622. https://doi.org/10.1016/j.jhazmat.2007.06.033.
(57) Zeng, L.; Li, X.; Liu, J. Adsorptive Removal of Phosphate from Aqueous Solutions Using Iron Oxide Tailings. *Water Res.* **2004**, *38* (5), 1318–1326. https://doi.org/10.1016/j.watres.2003.12.009.

Table of Contents Graphic